Crosshatching on $La_{0.5}Ca_{0.5}MnO_3$ ultrathin films epitaxially grown on $SrTiO_3(100)$

Zhi-Hong Wang,[1,2,*] O. I. Lebedev,[3,†] G. Van Tendeloo,[3] G. Cristiani,[2] and H.-U. Habermeier[2]
[1]*Beijing National Laboratory for Condensed Matter Physics, Institute of Physics, Chinese Academy of Sciences, P.O. Box 603, 100080 Beijing, China*
[2]*Max-Planck-Institut für Festköperforschung, Heisenbergstrasse 1, D-70569 Stuttgart, Germany*
[3]*Electron Microscopy for Materials Research (EMAT), University of Antwerp, Groenenborgerlaan 171, B2020 Antwerpen, Belgium*
(Received 28 May 2007; revised manuscript received 15 January 2008; published 18 March 2008)

The morphological evolution in $La_{0.5}Ca_{0.5}MnO_3/SrTiO_3(100)$ ultrathin films has been revealed by atomic force microscopy. It was found that ordered linear defects, which are in 1–2 unit cells high and oriented along the cubic [110] and [100] directions, first appear on the smooth surface of films with a thickness of 10 nm. As the epitaxial growth proceeds, these lines on surface develop into a crosshatch pattern for films with a thickness of 25 nm. Using the results of transmission electron microscopy and electrical measurements, we discuss the interplay between the surface pattern formation, the internal dislocation structure, and the variations in the electrical properties.

DOI: 10.1103/PhysRevB.77.115330 PACS number(s): 68.55.−a, 68.47.Gh, 68.37.−d, 81.16.Rf

In depositing material A on B through heteroepitaxy, the lattice misfit strain can induce a number of intriguing phenomena. The crosshatch pattern at the surface, observed in many heteroepitaxial semiconductor films such as SiGe/Si(100), is one of them and has invoked extensive interest in the past decades.[1–15] Recently, oxide electronics is becoming a promising scientific and technological area.[16,17] In film growth of perovskite oxides which possess rich functionalities, crosshatch surfaces were observed in $SrRuO_3$ thin films grown on $SrTiO_3$ (STO)(100) (Ref. 18) and in the heterostructure $(Ca_{1-x}Sr_x)(Zr_{1-x}Ru_x)O_3/SrRuO_3/STO(100)$.[19] However, apart from the above observations, there are no reports of crosshatch surfaces in other complex oxide films. In fact, in comparison with the intense work in semiconductor heteroepitaxy, the investigation of surface pattern formation in complex oxide films is just emerging. In this paper, we will show that the crosshatch surface can also appear in perovskite based manganite films. By exploiting atomic force microscopy (AFM), we will demonstrate the detailed morphological evolution in the heteroepitaxial films. Moreover, through transmission electron microscopy (TEM) and electrical measurements, we will reveal a tight correlation between the pattern formation, the dislocation nucleation, and the variations in film electrical properties.

As an example system, $La_{0.5}Ca_{0.5}MnO$ (LCMO)/STO(100) has been studied. Bulk LCMO is an orthorhombic perovskite with space group *Pnma*. Its lattice constants at room temperature are $a_o=5.4182$ Å, $b=7.6389$ Å, and $c=5.4269$ Å.[20] In a pseudocubic notation, the lattice constant $a_{LCMO}=1/2[d_{101}(3.834\ \text{Å})+d_{020}(3.819\ \text{Å})]=3.827$ Å, where d_{101} and d_{020} are the interplanar distances in the orthorhombic structure. The substrate STO is cubic with lattice constant $a=3.905$ Å. Hence, an in-plane tensile misfit $f=(a_{STO}-a_{LCMO})/a_{STO}\simeq 2\%$ is involved in the film epitaxy. Such a moderate misfit is propitious to reveal the morphological and structural evolution for a series of film thicknesses. On the other hand, for a thick LCMO film ($t\sim 160$ nm) grown on STO(100), Peng *et al.* ever found ordered three dimensional (3D) grain dots on the film surface.[21] It is thus important to explore how the film morphology evolves in the early stages of epitaxial growth. Therefore, in this study, we had paid extra attention to the growth of ultrathin films. It is also worth noting that the bulk LCMO is a well-known half-doped manganite which owns an antiferromagnetic-charge ordered state below ~150 K (upon cooling).[22–25] How the misfit strain and the strain relief modify the electrical properties in thin films is also an interesting question to study.

Ultrathin LCMO films with thicknesses of 5, 10, 15, and 25 nm were grown by pulsed laser deposition. High quality STO(100) with smooth terraces arising from a minor crystal miscut (~0.1°) were carefully chosen as the substrates. The film growth was performed at an oxygen pressure of 0.4 mbar with a substrate temperature of 850 °C. The laser fluence on the target was about 1.6 J/cm^2 and the ablation frequency was 5 Hz. After deposition, the thin film was *in situ* annealed at 900 °C for 15 min in 1 bar flowing oxygen. The θ-2θ x-ray diffraction (XRD) of the films was carried out on a Philips x-ray diffractometer with Cu $K\alpha$ radiation. It appears that above a film thickness of 10 nm, the film XRD peaks show sufficient intensity for analysis, indicating a (00l) orientation of the films. For simplicity, and also because of the fact that the LCMO films were found to be pseudocubic by the TEM analysis, the crystal indexing in the following will be referred to a cubic perovskite structure with lattice constant $a_c=3.8-3.9$ Å. A DI Nanoscope IIIa system working in taping mode was used to obtain the AFM images. The TEM study was carried out using a Jeol 4000EX electron microscope. Prior to the TEM work, the electrical resistance as a function of temperature and magnetic field for the films were measured by the standard four probe technique.

Figures 1(a)–1(d) display the AFM images and the film morphology. Both terraces and two dimensional (2D) islands are seen on the surface for each film, which indicates a coexistence of step flow and Frank–van der Merwe (layer by layer) growth. The surface for the ultrathin film with a thickness of 5 nm is atomically flat, having only a few 2D islands on the terraces. In contrast, the 10 nm thick film shows, besides the 2D islands on its surface, crystallographically oriented lines with a height of 1–2 unit cells. The lines running along [100] and [010] have a length of about 1–3 μm; those running along the orthogonal [110] directions generally ex-

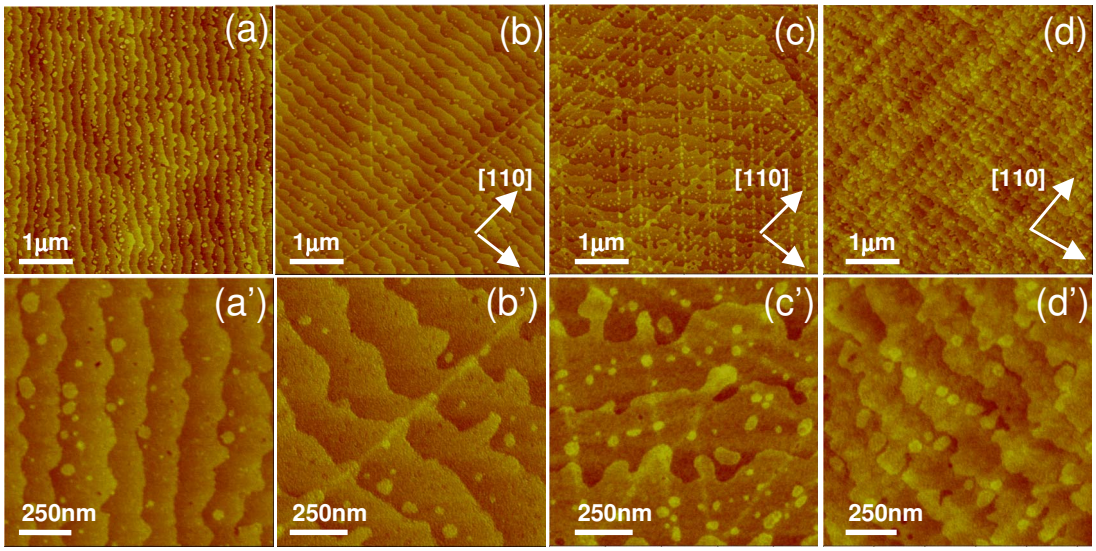

FIG. 1. (Color online) AFM images for the films with thicknesses of [(a) and (a′)] 5 nm, [(b) and (b′)] 10 nm, [(c) and (c′)] 15 nm, and [(d) and (d′)] 25 nm. The arrows indicate the cubic orthogonal [110] directions. The series in (a)–(d) are recorded in 5×5 μm^2, while (a′)–(d′) are images recorded in $\sim13\times1.3$ μm^2 from the local regions in (a)–(d), respectively.

ceed the scanning limit of about 15 μm. For thicker films ($t=15$ nm), in addition to the lines along ⟨110⟩, the lines in the ⟨100⟩ directions are developed as well. For films with a thickness of 25 nm, the dense lines are mainly along the two orthogonal [110] directions and the film surface exhibits a crosshatch pattern.

Figures 1(a′)–1(d′) show the AFM images recorded at a higher magnification corresponding to the local regions of Figs. 1(a)–1(d). The lines in the 10 nm thick film are well defined and the interaction between the line and the step edge creates an oriented fingertiplike structure. For the thicker films, the lines appear a bit fuzzy and the fingertiplike structure evolutes into a rectangular shape. It is also clear that, with an increasing line density, more and more 2D islands position themselves along the lines with a more or less constant lateral spacing.

The TEM study confirmed that all films were epitaxially grown with the crystallographic relation $(001)[100]_{LCMO}\|(100)[001]_{STO}$. Figure 2 shows representative cross-section high resolution TEM (HRTEM) images. Due to the tensile epitaxial strain, the film structure was found to be pseudocubic (R-3c) (Ref. 26) rather than the expected orthorhombic structure of the bulk material [see the Fourier transform pattern in the inset of Fig. 2(b)]. For the film with a thickness of 5 nm, the epitaxial growth is coherent from the interface to the upper surface. For the 15 nm thick film, although the perfect lattice is preserved [Fig. 2(b)], pure edge dislocations with a Burgers vector **b** parallel to the film plane were observed at the interface [Fig. 2(c)]. The formation of such misfit dislocations indicates that strain relaxation has already occurred in this film.

Figure 3(a) is a low magnification plan-view TEM image for the 15 nm thick film. The corresponding electron diffraction pattern clearly indicates a pseudocubic rather than an orthorhombic structure, as observed in the bulk material [see the inset of Fig. 3(a)]. One, therefore, can ignore a possible extrinsic strain relaxation induced in preparing the plan-view specimen. In accordance with the AFM measurements, ordered lines or strips propagating along the two orthogonal directions [010] and [100] were observed. Note the sequence of broad lines with dark contrasts parallel to [010]. The average lateral separation between them is consistent with that for the line pattern shown in the AFM image [Fig. 1(c)]. A closer look at the marked area in Fig. 3(a) shows that the broad lines consist of a set of partial dislocations or dislocation segments oriented along [110] [Fig. 3(b)]. HRTEM of a single line [Fig. 4(a)] clearly revealed the presence of almost periodically spaced threading dislocations with Burgers vectors $\mathbf{b}_1=a[100]$ [Fig. 4(b)] and $\mathbf{b}_2=a[110]$ [Fig. 4(c)]. It is interesting to note that the cores of the threading dislocations are not so compact or highly symmetric[27,28] but are somehow extended in the aligned [100] direction.

Generally, dislocations cannot end inside a bulk crystal. Because of the large lateral extension of the film compared to its thickness, it is very unlikely that each misfit dislocation would extend over the whole film; it will mostly be connected to the free surface by two arms of threading dislocations.[27,29–31] In other words, threading dislocations are concomitant with misfit dislocations. This explains why both of them were revealed by the TEM observations. Note that the surface of the 5 nm thick film is atomically flat, whereas on the surface of the 15 nm thick film, ordered lines and surface steps exist. The absence and presence of misfit dislocations in these two films, respectively, highlights a correlation between the surface line formation and the dislocation nucleation. The apparent similarities between the line patterns observed by AFM and plan-view TEM establish a concrete link between the threading dislocations and the crosshatched surface.

Because of the lattice discontinuity at the core, a threading dislocation is surrounded with an elastic stress field.[32] In the film growth, such a stress field interacts with the incoming adatoms so as to accommodate the excess elastic energy. This can result in a local preferential landing of adatoms on

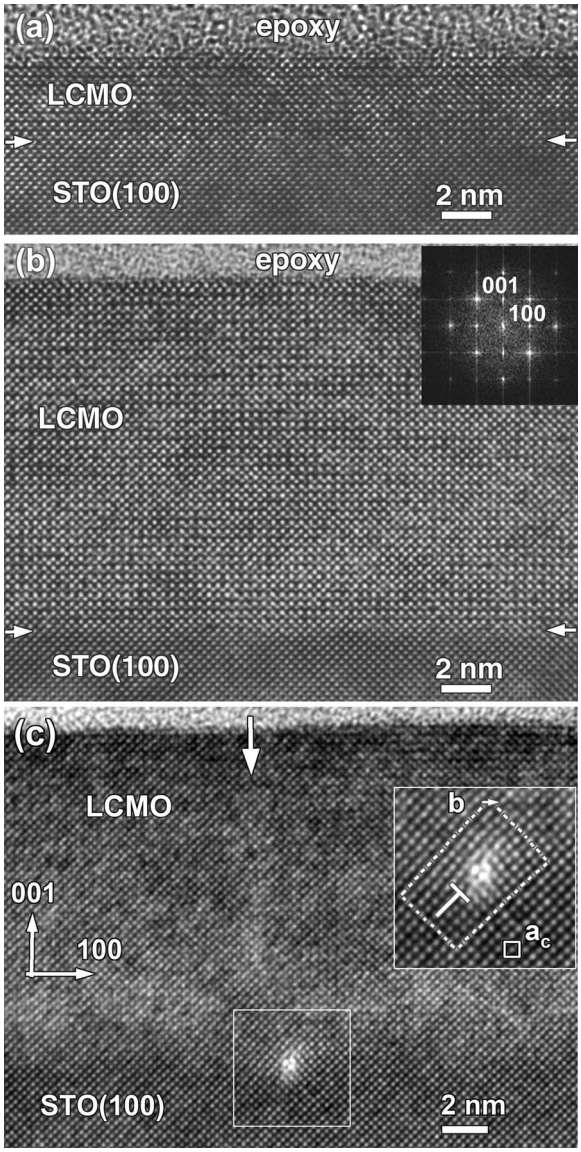

FIG. 2. Cross-section HRTEM images taken from films with thicknesses of (a) 5 nm and [(b) and (c)] 15 nm. The inset in (b) shows the Fourier transform of the image. The inset in (c) shows the Burgers circuit around the dislocation core; the small square with lattice constant a_c outlines the cubic perovskite unit cell.

the dislocation sites. At the critical thickness of 10 nm, the dislocations just seem to relax the misfit strain. It is possible that the line consisting of arrays of threading dislocations (as shown in Fig. 3) is rather narrow for this film. Hence, the associated strain field does not attract much adatoms to form sizable 2D islands along the line. On the other hand, however, since the step flow growth is involved in this film, the narrow-scaled strain field interacts with the step edge, producing a fingertiplike feature at the step edge, as shown in Figs. 1(b) and 1(b′). As the film growth proceeds, more misfit dislocations are created. When the interior misfit dislocations become regularly arranged due to the mutual interaction (repulsive and/or attractive), the threading dislocations at the surface will accordingly become configured into an ordered line network with a broad linewidth, as observed by

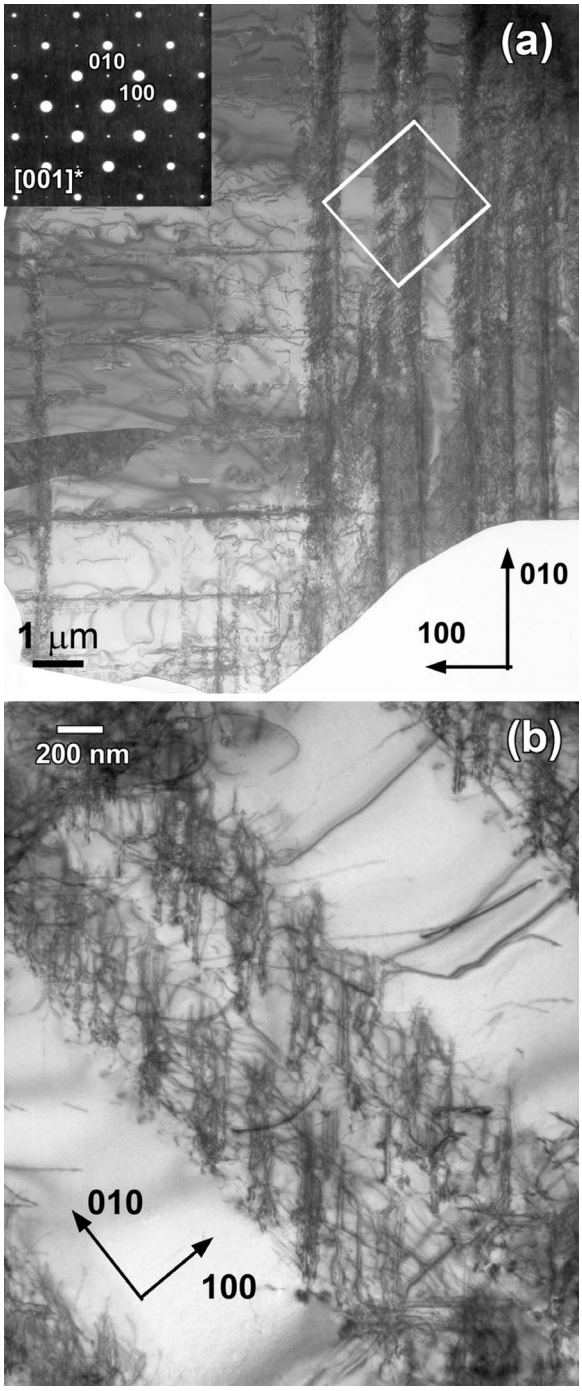

FIG. 3. (a) Low magnification plan-view TEM image of crosshatch lines along the two orthogonal directions [010] and [100] taken from a 15 nm thick film. (b) Magnified area of two dark contrast lines in (a) marked by a white rectangle. Note that the lines consist of a set of ordered dislocations parallel to [110]. The inset in (a) shows the corresponding electron diffraction pattern.

the plan-view TEM. It is plausible to expect that those broad lines and, particularly, the cross intersections in the network readily break up the coherence of the step flow growth and promote the nucleations of 2D islands. Eventually, at a film thickness of 25 nm, these numerous aligned 2D islands give rise to a crosshatch pattern in the overall view.

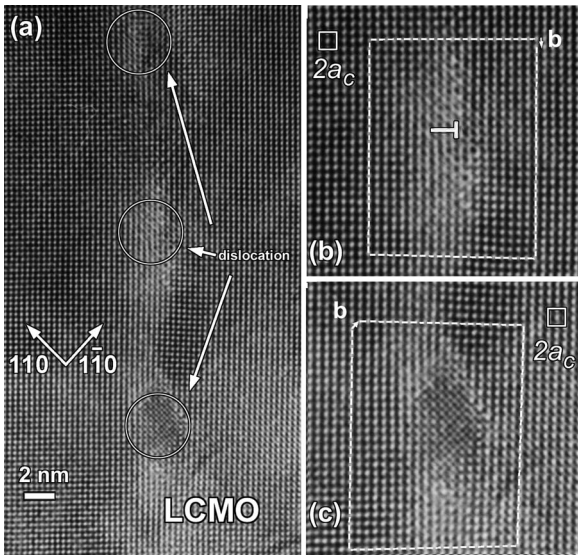

FIG. 4. Plan-view HRTEM images taken from the 15 nm thick film. The white lines in the enlargements (b) and (c) outline the Burgers circuit around the dislocation core.

It should be pointed out that besides the above adatom processes affected by the strain field, slip steps created by the glide of dislocations could be an alternative explanation for the crosshatch pattern.[3,4] Nevertheless, for the current LCMO films, the misfit dislocations have a Burgers vector parallel to the interface. These dislocations cannot be formed by glide but only by vertical climb via the removal of atoms by absorption of vacancies or by the emission of atoms to the free layer surface.[33] Furthermore, the specific surface wavelike deformation associated with the surface slip steps[34] was not observed in our AFM measurements. These facts suggest that the present crosshatch can indeed be attributed to the above surface adatom processes. Note that, for the ultrathin films, we only considered the misfit strain caused by the lattice mismatch between the film and substrate. If the film thickness increases, the thermal expansion mismatch between film and substrate will impart an additional lattice misfit to the film epitaxy.[21] The lattice misfit from a moderate to an enhanced amplitude can result in a 2D to 3D growth mode transition.[34] This could be the reason for the tendency to form ordered grain arrays on the surface of a thick LCMO film.[21]

Figure 5 shows the temperature dependence of the resistivity measured at zero magnetic field. All films show a semiconducting behavior, but no resistance jump[22,23] was detected neither on cooling nor on warming. This implies that an antiferromagnetic state could be retained in these thin films. The charge ordered state in the bulk material, however, is suppressed by the biaxial tensile strain. Figure 6 shows the magnetoresistance (MR) ratio versus external magnetic field (H) measured at 120 K. The MR is defined as $\mathrm{MR}=[R(H)-R(0)]/R(0)$, where $R(0)$ is the resistance at zero field. It is interesting to find that the MR(H) curve displays a paraboliclike behavior and the MR at high field appears to increase with the film thickness. Because the dislocations formed in strain relief locally alter the stoichiometry and the related

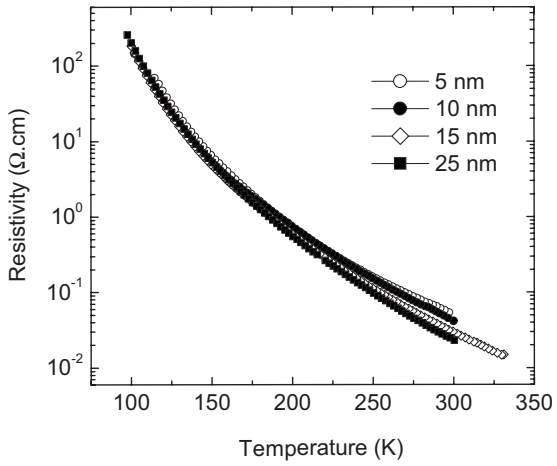

FIG. 5. Temperature dependence of resistivity of the LCMO films measured at zero field. The thin films from $t=5$ to 15 nm were measured in cooling and the 25 nm thick film was measured on heating.

electronic structure,[35,36] these line defects (particularly the threading dislocations) could generate more conducting filaments in the antiferromagnetic matrix. Note that the paraboliclike MR(H) behavior with $\partial^2 MR/\partial H^2 < 0$ at low fields shown in Fig. 6 is usually found above the Curie temperature for ferromagnetic perovskite manganites.[37–39] We infer that the induced filaments are in a paramagnetic state at 120 K. Upon applying an external field, the disordered spins in the filaments will tend to align, which reduces the resistance and thus brings about a marked MR.[40] There are more dislocations nucleating in the thicker films; therefore, the MR is found to increase with the film thickness and, in fact, the significant increase in the density of the surface lines from $t=10$ to 15 nm corresponds well to a sudden increase in MR, as shown in the inset of Fig. 6.

In summary, a surface crosshatching has been observed and analyzed in LCMO ultrathin films epitaxially grown on STO(100). It was found that the nucleation of dislocations, particularly the threading dislocations, plays a crucial role in the formation of the crosshatch surface. The present work

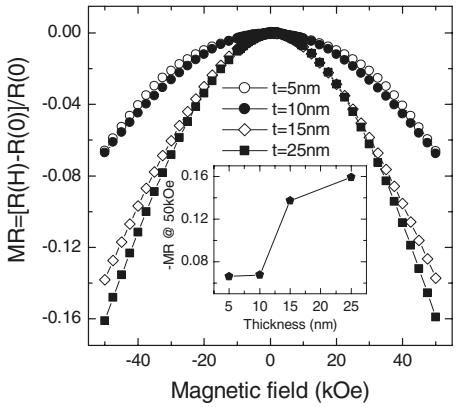

FIG. 6. Magnetoresistance ratio vs external magnetic field of the LCMO films measured at 120 K. The inset plots the MR at 50 kOe vs the film thickness.

together with the previous studies[18,19,21] suggests that, though chemical and crystallographic complexities exist in perovskite oxides, the universal strain relaxation due to the lattice misfit between the film and substrate can lead to simple structural ordering (morphological and interior). It should be interesting to expand the research to the heteroepitaxy of other perovskite oxides. First, one can exploit the self-patterned film surfaces as templates for the fabrication of novel oxide nanostructures. This technique has been proved to be fruitful in semiconductor films. Second, as demonstrated by the modification in magnetoresistance, the ordered dislocations buried under the crosshatch surface can be treated as an effective element for tailoring the film physical properties.

The authors are grateful to E. Brücher, G. Götz, H. Zhang, and B. Lemke for technical support. One of the authors (Z.-H.W.) is grateful to X. F. Duan at IOP, CAS, for discussions. Part of this work was performed with the financial support from the European Union under the Framework 6 program under a contract for an Integrated Infrastructure Initiative (Reference No. 026019 ESTEEM).

*wangzh@g203.iphy.ac.cn
†oleg.lebedev@ua.ac.be

[1] S. Kishino, M. Ogirima, and K. Kurata, J. Electrochem. Soc. **119**, 617 (1972).
[2] J. W. P. Hsu, E. A. Fitzgerald, Y. H. Xie, P. J. Silverman, and M. J. Cardillo, Appl. Phys. Lett. **61**, 1293 (1992).
[3] S. Yu. Shiryaev, F. Jensen, and J. W. Petersen, Appl. Phys. Lett. **64**, 3305 (1994).
[4] M. A. Lutz, R. M. Feenstra, F. K. LeGoues, P. M. Mooney, and J. O. Chu, Appl. Phys. Lett. **66**, 724 (1995).
[5] M. Albrecht, S. Christiansen, J. Michler, W. Dorsch, H. P. Strunk, P. O. Hansson, and E. Bauser, Appl. Phys. Lett. **67**, 1232 (1995).
[6] T. Pinnington, C. Lavoie, T. Tiedje, B. Haveman, and E. Nodwell, Phys. Rev. Lett. **79**, 1698 (1997).
[7] R. Hammond, P. J. Phillips, T. E. Whall, E. H. C. Parker, T. Graf, H. Von Känel, and A. J. Shields, Appl. Phys. Lett. **71**, 2517 (1997).
[8] A. M. Andrews, A. E. Romanov, J. S. Speck, M. Bobeth, and W. Pompe, Appl. Phys. Lett. **77**, 3740 (2000).
[9] H. Chen, Y. K. Li, C. S. Peng, H. F. Liu, Y. L. Liu, Q. Huang, J. M. Zhou, and Q. K. Xue, Phys. Rev. B **65**, 233303 (2002).
[10] X. L. Yuan, T. Sekiguchi, J. Niitsuma, Y. Sakuma, S. Ito, and S. G. Ri, Appl. Phys. Lett. **86**, 162102 (2005).
[11] H. Chen, F. Chen, X. M. Wang, X. K. Yu, J. R. Liu, K. B. Ma, W. K. Chu, H. H. Cheng, I. S. Yu, Y. T. Ho, and K. Y. Horng, Appl. Phys. Lett. **87**, 103504 (2005).
[12] S. Yu. Shiryaev, F. Jensen, and J. W. Petersen, Appl. Phys. Lett. **64**, 13 (1994).
[13] J. W. P. Hsu, E. A. Fitzgerald, Y. H. Xie, and P. J. Silverman, J. Appl. Phys. **79**, 7743 (1996).
[14] M. H. Gray and J. W. P. Hsu, Appl. Phys. Lett. **76**, 1294 (2000); M. H. Gray, J. W. P. Hsu, L. Giovane, and M. T. Bulsara, Phys. Rev. Lett. **86**, 3598 (2001).
[15] K. Sawano, S. Koh, Y. Shiraki, N. Usami, and K. Nakagawa, Appl. Phys. Lett. **83**, 4339 (2003).
[16] *Thin Films and Heterostructures for Oxide Electronics*, edited by S. B. Ogale (Springer, New York, 2005).
[17] A. P. Ramirez, Science **315**, 1377 (2007).
[18] F. Sánchez, U. Lüders, G. Herranz, I. C. Infante, J. Fontcuberta, M. V. García-Cuenca, C. Ferrater, and M. Varela, Nanotechnology **16**, S190 (2005).
[19] S. G. Kim, Y. Wang, and I. W. Chen, Appl. Phys. Lett. **89**, 031905 (2006).
[20] P. M. Woodward, T. Vogt, D. E. Cox, A. Arulraj, C. N. R. Rao, P. Karen, and A. K. Cheetham, Chem. Mater. **10**, 3652 (1998).
[21] H. B. Peng, B. R. Zhao, Z. Xie, Y. Lin, B. Y. Zhu, Z. Hao, H. J. Tao, B. Xu, C. Y. Wang, H. Chen, and F. Wu, Phys. Rev. Lett. **82**, 362 (1999).
[22] P. G. Radaelli, D. E. Cox, M. Marezio, S.-W. Cheong, P. E. Schiffer, and A. P. Ramirez, Phys. Rev. Lett. **75**, 4488 (1995).
[23] P. S. Schiffer, A. P. Ramirez, W. Bao, and S.-W. Cheong, Phys. Rev. Lett. **75**, 3336 (1995).
[24] C. H. Chen and S.-W. Cheong, Phys. Rev. Lett. **76**, 4042 (1996).
[25] A. P. Ramirez, P. Schiffer, S.-W. Cheong, C. H. Chen, W. Bao, T. T. M. Palstra, P. L. Gammel, D. J. Bishop, and B. Zegarski, Phys. Rev. Lett. **76**, 3188 (1996).
[26] O. I. Lebedev, G. Van Tendeloo, S. Amelinckx, F. Razavi, and H.-U. Habermeier, Philos. Mag. A **81**, 797 (2001).
[27] T. Suzuki, Y. Nishi, and M. Fujimoto, Philos. Mag. A **79**, 2461 (1999).
[28] I. B. Misirlioglu, A. L. Vasiliev, M. Aindow, S. P. Alpay, and R. Ramesh, Appl. Phys. Lett. **84**, 1742 (2004).
[29] H. Ibach, *Physics of Surfaces and Interfaces* (Springer, Berlin, 2006).
[30] J. W. Matthews, J. Vac. Sci. Technol. **12**, 126 (1975).
[31] R. People and J. C. Bean, Appl. Phys. Lett. **47**, 322 (1985).
[32] A. Nakamura, K. Matsunaga, J. Tohma, T. Yamamoto, and Y. Ikuhara, Nat. Mater. **2**, 453 (2003).
[33] G. Springholz and K. Wiesauer, Phys. Rev. Lett. **88**, 015507 (2001).
[34] G. Springholz, G. Bauer, and V. Holy, Phys. Rev. B **54**, 4500 (1996).
[35] C. L. Jia, A. Thust, and K. Urban, Phys. Rev. Lett. **95**, 225506 (2005).
[36] K. Szot, W. Speier, G. Bihlmayer, and R. Waser, Nat. Mater. **5**, 312 (2006).
[37] J. O'Donnell, M. Onellion, M. S. Rzchowski, J. N. Eckstein, and I. Bozovic, Phys. Rev. B **54**, R6841 (1996).
[38] J. Fontcuberta, B. Martínez, A. Seffar, S. Piñol, J. L. García-Muñoz, and X. Obradors Phys. Rev. Lett. **76**, 1122 (1996).
[39] H. L. Ju and H. Sohn, Solid State Commun. **102**, 463 (1997).
[40] P. Wagner, I. Gordon, L. Trappeniers, J. Vanacken, F. Herlach, V. V. Moshchalkov, and Y. Bruynseraede, Phys. Rev. Lett. **81**, 3980 (1998).